Periodic Fast Radio Bursts as a Probe of Extragalactic Asteroid Belts

Z. G. Dai[1,2] and S. Q. Zhong[1,2]
[1] School of Astronomy and Space Science, Nanjing University, Nanjing 210023, People's Republic of China; dzg@nju.edu.cn
[2] Key Laboratory of Modern Astronomy and Astrophysics (Nanjing University), Ministry of Education, Nanjing, People's Republic of China

Abstract

The periodic activity of the repeating fast radio burst (FRB) 180916.J0158+65 was recently reported by the CHIME/FRB Collaboration team. From this source 28 bursts not only show a ∼16 day period with an active phase of ∼4.0 days, but they also exhibit a broken power law in differential energy distribution. In this Letter, we suggest that FRB 180916.J0158+65-like periodic FRBs could provide a unique probe of extragalactic asteroid belts (EABs), based on our previously proposed pulsar-EAB impact model, in which repeating FRBs arise from an old-aged, slowly spinning, moderately magnetized pulsar traveling through an EAB around another stellar-mass object. These two objects form a binary, and thus the observed period is in fact the orbital period. We show that this model can be used to well interpret all of the observed data of FRB 180916.J0158+65. Furthermore, we constrain the EAB's physical properties and find that (1) the outer radius of the EAB is at least an order of magnitude smaller than that of its analog in the solar system, (2) the differential size distribution of the EAB's asteroids at small diameters (large diameters) is shallower (steeper) than that of solar system small objects, and (3) the two belts have a comparable mass.

Unified Astronomy Thesaurus concepts: Radio bursts (1339); Asteroids (72); Minor planets (1065); Radio continuum emission (1340); Neutron stars (1108)

1. Introduction

Since they were discovered for the first time (Lorimer et al. 2007), fast radio bursts (FRBs) have become one of the most mysterious astrophysical transients, because their physical origin remains unknown (Cordes & Chatterjee 2019; Petroff et al. 2019; Platts et al. 2019; Katz 2020). To date, at least 100 FRB sources have been detected, among which ∼20 sources show the repeating behavior (see also the catalog[3]). The discovery of the first repeating source FRB 121102 (Spitler et al. 2014) and the long-term follow-up observations (Scholz et al. 2016; Spitler et al. 2016; Chatterjee et al. 2017; Marcote et al. 2017) indicate that all of the bursts from this source have a temporally clustering feature, providing an important clue to understanding a possible origin of FRBs.

Recently, the CHIME/FRB Collaboration team claimed to discover a periodically repeating source, FRB 180916.J0158 +65, at ∼600 MHz (CHIME/FRB Collaboration et al. 2020). This source is harbored in a massive spiral galaxy at redshift $z = 0.0337 \pm 0.0002$ (Marcote et al. 2020), implying a luminosity distance $D_L = 149.0 \pm 0.9$ Mpc for the Hubble constant $H_0 = 67.8$ km s^{-1} Mpc^{-1}. They detected 28 bursts from 2018 September 16 to 2019 October 30 and found a period of 16.35 ± 0.18 days with an active phase of ∼4.0 days (CHIME/FRB Collaboration et al. 2020). The average burst rate is $\mathcal{R}_{FRB} \sim 25$ yr^{-1}. In addition, the differential energy distribution of all of the bursts from this source reveals two power laws with indices of -1.2 ± 0.3 and -2.5 ± 0.5, connecting at a fluence ∼6.3 Jy ms (i.e., an isotropic-equivalent radio emission energy ∼1.0×10^{38} erg, CHIME/FRB Collaboration et al. 2020). A similar energy distribution can be seen for FRB 121102 with different radio telescopes (for statistical analyses, see Gourdji et al. 2019; Wang & Zhang 2019; Lin & Sang 2020; Oostrum et al. 2020). This shows that a turnover in

the energy distribution of repeating FRBs seems to exist generally, suggesting that it may be intrinsic.

Several models were proposed to explain the periodic activity of FRB 180916.J0158+65. In the first type of model, the ∼16 day period is due to magnetar-free precession (Levin et al. 2020; Zanazzi & Lai 2020), orbit-induced spin precession (Yang & Zou 2020), or fallback disk-induced precession (Tong et al. 2020). The basis of these studies is the early suggestion that repeating FRBs could originate from the magnetic activity of a magnetar (Popov & Postnov 2013; Lyubarsky 2014; Katz 2016; Murase et al. 2016; Beloborodov 2017; Kashiyama & Murase 2017; Kumar et al. 2017; Metzger et al. 2017, 2019). The second type of model argued that the observed period is attributed to a binary period but the bursts could result from the distorted magnetic field lines of a pulsar immersed in a strong stellar wind of a massive companion (Ioka & Zhang 2020), following the cosmic combing model (Zhang 2017, 2018). A similar binary system scenario with a different bursting mechanism was proposed by Lyutikov et al. (2020) and Gu et al. (2020). All of the works did not discuss an energy distribution of the repeating bursts from FRB 180916.J0158 +65 within the frame of a pulsar.

In this Letter, we suggest that FRB 180916.J0158+65-like periodic FRBs could provide a unique probe of extragalactic asteroid belts (EABs). Debris disks including asteroidal objects and their belts are widely thought to be the remains of the planet formation process. This is currently one of the most interesting topics in astronomy. The motivation of our study is based on the model of Dai et al. (2016), in which repeating FRBs originate from an old-aged, slowly spinning, moderately magnetized pulsar traveling through an EAB around another stellar-mass object (possibly a star, a white dwarf, or a neutron star). Interestingly, if the two objects form a binary, then temporally clustering and even periodically repeating bursts would be naturally expected in this model, as discussed in Dai et al. (2016) and Bagchi (2017) for FRB 121102. Furthermore,
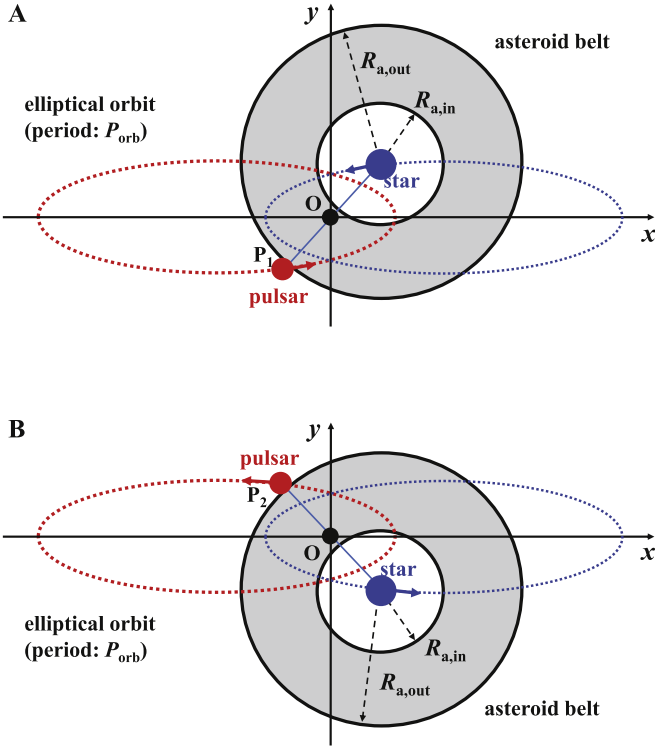
---

[3] http://www.frbcat.org

A

B

Figure 1. Schematic picture of pulsar-EAB collisions. An old pulsar and a star with an EAB form a binary and rotate around their center of mass (point O), which is taken to be the original point of a coordinate system (x, y). The two objects move along respective elliptical orbits with an orbital period P_{orb}. These orbits are assumed to be coplanar with the belt in order that pulsar-asteroid collisions are the most frequent. The pulsar first arrives at point P_1, at which it exactly enters the belt (panel A), and subsequently the pulsar reaches point P_2, at which it is just leaving from the EAB (panel B). The inner radius of the EAB is $R_{a,in}$.

based on this model, observable radio bursts in the Milky Way galaxy were also predicted to arise from collisions between neutron stars and interstellar asteroids (Siraj & Loeb 2019). The remaining part of this Letter is organized as follows. In Section 2 we constrain the physical properties (outer radius, mass, and asteroidal size distribution) of an EAB by using the observed data of FRB 180916.J0158+65. We present discussion and conclusions in Sections 3 and 4, respectively.

2. Constraints on an EAB

Following Dai et al. (2016), we assume that a slowly spinning ($P_{pulsar} \gtrsim 1$ s), moderately magnetized, wandering pulsar with an age $t_{pulsar} \gtrsim 10^7$ yr is captured by another stellar-mass object with a disk-shaped EAB of an outer radius $R_{a,out}$. This EAB has an inner radius $R_{a,in}$ and an orbital inclination angle,[4] implying that its thickness is nearly proportional to radius. In structure, the EAB may thus be analogous to the main asteroid belt in the solar system (DeMeo & Carry 2014; Peña et al. 2020) but the two belts could have some different physical parameters. The pulsar and the star, whose masses are taken to be M_{pulsar} and M_{star}, respectively, form a binary (see Figure 1) and rotate around the center of mass (i.e., point O), which is also assumed to be the original

---
[4] In the solar system, the main asteroid belt's inner radius $R_{a,in} \sim 2.0$ au, outer radius $R_{a,out} \sim 3.3$ au, and orbital inclination angle $\theta_{a,incl} \sim 20°$ (DeMeo & Carry 2014), so that the belt's thickness factor $\eta_t = 2 \times \sin\theta_{a,incl} \sim 0.7$ and width factor $\eta_w = (R_{a,out} - R_{a,in})/R_{a,out} \sim 0.4$.

point of a coordinate system (x, y). The two objects move along respective elliptical orbits with a period P_{orb}. In the following, we investigate some constraints on the physical properties of the EAB by using the observed data of FRB 180916. J0158+65.

2.1. Constraint on the Outer Radius

In order to make pulsar-asteroid collisions the most frequent, we here consider a simple case in which the pulsar's elliptical orbit and the EAB are coplanar.[5] The lengths of the semimajor and semiminor axes of the pulsar's elliptical orbit are a and b, respectively, which are related with an orbital eccentricity through $e = (a^2 - b^2)^{1/2}/a$. For FRB 180916.J0158+65, from Kepler's third law, the length a for the pulsar is given by

$$a = [G(M_{pulsar} + M_{star})]^{1/3}\left(\frac{P_{orb}}{2\pi}\right)^{2/3}\left(\frac{1}{1+q}\right)$$
$$= 2.7 \times 10^{12}(1+q)^{-2/3}\hat{M}_{star}^{1/3}\hat{P}_{orb}^{2/3} \text{ cm,} \qquad (1)$$

where $q \equiv M_{pulsar}/M_{star}$ is the mass ratio of the two objects, $\hat{M}_{star} = M_{star}/1.4\,M_\odot$, and $\hat{P}_{orb} = P_{orb}/16.35$ days. The two elliptical orbits satisfy

$$\frac{(x + ea)^2}{a^2} + \frac{y^2}{b^2} = 1, \qquad (2)$$

and

$$\frac{(x - eqa)^2}{(qa)^2} + \frac{y^2}{(qb)^2} = 1, \qquad (3)$$

which correspond to the pulsar and the star, respectively.

As shown in panel A of Figure 1, when the star is at point $(x_{star}, y_{star}$; where it is required that $x_{star} > 0$ and $y_{star} > 0$), the pulsar reaches point P_1, whose coordinates are $(-x_{star}/q, -y_{star}/q)$, at which the pulsar happens to arrive at a circular outer boundary of the EAB. Because this outer boundary satisfies the following equation

$$(x - x_{star})^2 + (y - y_{star})^2 = R_{a,out}^2, \qquad (4)$$

when the pulsar reaches point P_1 the coordinates of its position are found from

$$x_{star}^2 + y_{star}^2 = \left(\frac{q}{1+q}\right)^2 R_{a,out}^2, \qquad (5)$$

and

$$\frac{(x_{star} - eqa)^2}{(qa)^2} + \frac{y_{star}^2}{(qb)^2} = 1. \qquad (6)$$

From Equations (5) and (6), thus, we can obtain (x_{star}, y_{star}) if three parameters e, q, and $R_{a,out}$ are given. In addition, we can also see from panel B of Figure 1 that when the star reaches point $(x_{star}, -y_{star})$, the pulsar is just leaving from the EAB, at which time the coordinates of the pulsar's position become $(-x_{star}/q, y_{star}/q)$, namely point P_2.

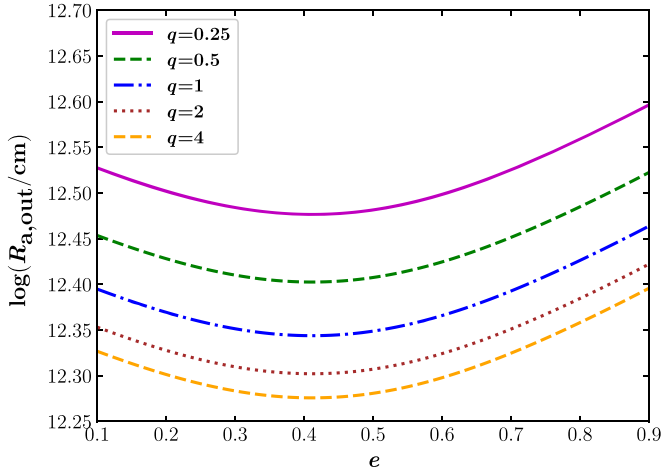[5] Please see the second discussion on the probability of this case in Section 3.

Figure 2. $R_{a,out}$ as a function of e for $M_{pulsar} = 1.4\,M_\odot$ and $q = 0.25, 0.5, 1, 2,$ and 4, in the case of FRB 180916.J0158+65 with an orbital period $P_{orb} = 16.35$ days and a duty cycle $\zeta = 0.24$ (taken from CHIME/FRB Collaboration et al. 2020).

The area swept out by a line between the pulsar and the center of mass from point P_1 to P_2 is calculated by

$$\Delta S_{pulsar} = \frac{1}{2} \int_{-\theta_1}^{+\theta_2} r^2 d\theta = \int_0^{\theta_2} \left[\frac{a(1 - e^2)}{1 + e\cos\theta} \right]^2 d\theta, \quad (7)$$

where θ_1 (or θ_2) is the angle between the x-axis and the line OP_1 (or OP_2), $\theta_1 = \theta_2 = \pi - \arctan(y_{star}/x_{star})$. The total area enclosed by the pulsar's elliptical orbit is $S_{pulsar} = \pi(1 - e^2)^{1/2} a^2$. According to Kepler's second law, the ratio of these two areas is equal to the duration of the active time window ($\Delta P_{orb} = 4$ days), in which the pulsar moves from point P_1 to P_2, divided by P_{orb}. This means the duty cycle

$$\zeta \equiv \frac{\Delta S_{pulsar}}{S_{pulsar}} = \frac{\Delta P_{orb}}{P_{orb}} = \frac{4}{16.35} = 0.24. \quad (8)$$

Therefore, under the condition of Equation (8), together with Equations (5)–(7), we can numerically calculate $R_{a,out}$ as a function of e if the parameter q is known. Figure 2 shows $R_{a,out}$ versus e for $M_{pulsar} = 1.4\,M_\odot$ and five fixed values of q. We can see from this figure that $R_{a,out}$ varies slowly with e and has the minimum value at $e \sim 0.42$ for a given q. The outer radius increases from ~ 0.13 au to ~ 0.26 au if q is set to be 0.25 to 4. This shows that $R_{a,out}$ of the EAB responsible for FRB 180916. J0158+65 is at least an order of magnitude smaller than that of its solar system analog (DeMeo & Carry 2014; Peña et al. 2020).

2.2. Constraint on the Asteroidal Size Distribution

Here we consider an asteroid-pulsar collision. Following Colgate & Petscheck (1981), we assume that an asteroid as a solid body falls freely in the pulsar's gravitational field. This asteroid is originally approximated by a sphere with a mass m. It will first be distorted tidally by the pulsar at some break-up radius and subsequently elongated in the radial direction and compressed in the transverse direction. The timescale of such a bar-shaped asteroid accreted on the pulsar's surface is estimated by $\Delta t \simeq 1.6 m_{18}^{4/9}$ ms, where $m_{18} = m/10^{18}$ g (see Equation (2) of Dai et al. 2016). This timescale is not only independent of the pulsar's radius but also weakly dependent

on the other parameters such as the pulsar's mass and the asteroidal tensile strength and original mass density, even though the asteroid is assumed to be mainly composed of iron-nickel nuclei. The average rate of gravitational energy release near the stellar surface during Δt is approximated by $\dot{E}_G \simeq G m M_{pulsar}/(R_{pulsar} \Delta t) = 1.2 \times 10^{41} m_{18}^{5/9}$ erg s^{-1}, where and hereafter $M_{pulsar} = 1.4\,M_\odot$ and the pulsar's radius $R_{pulsar} = 10^6$ cm are adopted. These simple estimates of Δt and $\dot{E}_G$ are well consistent with the observations of FRBs. This is why asteroid-pulsar collisions have been proposed as an origin model of FRBs (Geng & Huang 2015; Dai et al. 2016). We now discuss the asteroidal size distribution in two following ways.

2.2.1. A Simple Way

We assume that ξ is the efficiency of converting gravitational energy to radio emission and $f = \Delta\Omega/(4\pi)$ is the beaming factor of the emission (where $\Delta\Omega$ is the corresponding solid angle), so the isotropic-equivalent energy of an FRB can be estimated by

$$E_{iso} \simeq (\xi/f)\dot{E}_G \Delta t = 1.9 \times 10^{38} (\xi/f) m_{18} \text{ erg.} \quad (9)$$

This linearly proportional relation can provide an energy distribution of FRBs if both ξ and f are constants.

As shown by the Sloan Digital Sky Survey data (Ivezić et al. 2001; Davis et al. 2002), the Subaru Main Belt Asteroid Survey data (Yoshida & Nakamura 2007), the Spitzer Space Telescope infrared data (Ryan et al. 2015), and the High cadence Transient Survey data (Peña et al. 2020) of solar system objects, the differential size distribution of the EAB's asteroids can be assumed to be written as

$$\frac{dN}{dD} \propto D^{-\beta} \propto \begin{cases} D^{-\beta_1}, & D < D_{br}, \\ D^{-\beta_2}, & D \geqslant D_{br}, \end{cases} \quad (10)$$

where D is the asteroidal diameter. In the solar system main belt, $\beta_1 \simeq 2.3$, $\beta_2 \simeq 4.0$ and $D_{br} \sim 6.0$ km (Ivezić et al. 2001; Davis et al. 2002; Yoshida & Nakamura 2007; Ryan et al. 2015; Yoshida et al. 2019; Peña et al. 2020). A similar size distribution for Jupiter Trojans and Hildas was recently shown by Yoshida et al. (2019). These authors comparatively studied the size frequency distributions of Jupiter Trojans, Hildas, and main belt asteroids, and suggested that some physical mechanisms including collisional evolution and/or Yarkovsky effect during planet migration at the early solar system could provide a clue for understanding the origin of Equation (10). In the case of $E_{iso} \propto m$, this equation leads to a differential energy distribution of radio bursts,

$$\frac{dN}{dE_{iso}} \propto E_{iso}^{-\alpha} \propto \begin{cases} E_{iso}^{-\alpha_1}, & E_{iso} < E_{br}, \\ E_{iso}^{-\alpha_2}, & E_{iso} \geqslant E_{br}, \end{cases} \quad (11)$$

where $\alpha = (\beta + 2)/3$ and the break energy $E_{br} \sim 1.7 \times 10^{38}(\xi/f)(D_{br}/6 \text{ km})^3$ erg is derived from Equation (9).

For FRB 180916.J0158+65, $\alpha_1 = (\beta_1 + 2)/3 \simeq 1.2$, $\alpha_2 = (\beta_2 + 2)/3 \simeq 2.5$, and $E_{br} \sim 1.0 \times 10^{38}$ erg (calculated from Extended Data Figure 3 of CHIME/FRB Collaboration et al. 2020). These data imply that $\beta_1 \simeq 1.6$, $\beta_2 \simeq 5.5$, and $D_{br} \sim 5.0(\xi/f)^{-1/3}$ km. Therefore, the differential size distribution of the EAB's asteroids at small diameters (large

diameters) is shallower (steeper) than that of asteroidal objects in the solar system.

2.2.2. A Realistic Way

Dai et al. (2016) explored asteroid-pulsar impact and radiation physics in detail and found that, during such an impact, an electric field induced outside of the asteroid has such a strong component parallel to the stellar magnetic field that electrons are torn off the asteroidal surface and accelerated to ultra-relativistic energies instantaneously. Subsequent movement of these electrons along magnetic field lines will cause coherent curvature radiation. From Equation (15) of Dai et al. (2016), the isotropic-equivalent emission luminosity is estimated by

$$L_{\rm iso} \sim 2.6 \times 10^{40} (f\rho_{\rm c,6})^{-1} m_{18}^{8/9} \mu_{30}^{3/2} \ {\rm erg \ s^{-1}}, \quad (12)$$

where the beaming factor f is introduced, $\rho_{\rm c,6}$ is the curvature radius of a magnetic field line near the stellar surface in units of 10^6 cm, μ_{30} is the pulsar's magnetic dipole moment in units of 10^{30} G cm^3, and the other parameters are taken for an iron-nickel asteroid (also refer to Equation (1) of Siraj & Loeb 2019). Thus, the isotropic-equivalent energy of an FRB is estimated by

$$E_{\rm iso} \simeq L_{\rm iso}\Delta t \sim 4.1 \times 10^{37} (f\rho_{\rm c,6})^{-1} m_{18}^{4/3} \mu_{30}^{3/2} \ {\rm erg}. \quad (13)$$

This equation leads to an energy distribution of FRBs being similar to Equation (11) but $\alpha = (\beta + 3)/4$ and $E_{\rm br} \sim 3.6 \times 10^{37} (f\rho_{\rm c,6})^{-1} (D_{\rm br}/6 \ {\rm km})^4 \mu_{30}^{3/2}$ erg.

As clarified in CHIME/FRB Collaboration et al. (2020), only the CHIME/FRB telescopes detected radio bursts along the direction of FRB 180916.J0158+65 (and meanwhile, the 100 m Effelsberg telescope did not detect any bursts). This implies that the typical emission frequency of an FRB from this source is $\sim$600 MHz, which requires

$$\mu_{30}^{3/2} \rho_{\rm c,6} \sim 10\chi^3, \quad (14)$$

where $\chi \lesssim 1$ is introduced by assuming that $\chi\gamma_{\rm max}$ is the typical Lorentz factor of ultra-relativistic electrons emitting the FRB. Equation (14) is derived from the maximum Lorentz factor ($\gamma_{\rm max}$) and curvature radiation frequency ($\nu_{\rm curv} \sim 600$ MHz) of electrons given by Equations (12) and (14) of Dai et al. (2016), respectively.

From Equations (10) and (11), we can see that $\beta_1 \simeq 1.8$, $\beta_2 \simeq 7.0$, and $D_{\rm br} \sim 7.6 f^{1/4} \rho_{\rm c,6}^{1/4} \mu_{30}^{-3/8}$ km $\sim 5.7 f^{1/4} \chi_{-0.5}^{3/4} \mu_{30}^{-3/4}$ km, where $\chi_{-0.5} = \chi/10^{-0.5}$ and Equation (14) has been used. These results are basically consistent with the simple estimates in Section 2.2.1.

2.3. Constraint on the Belt's Total Mass

As the geometric structure of the EAB may be somewhat similar to that of the solar system main asteroid belt, we obtain the EAB's volume, $V_{\rm belt} \sim 2\pi\eta_{\rm t}\eta_{\rm w}R_{\rm a,out}^3$, where $\eta_{\rm t}$ and $\eta_{\rm w}$ are assumed to be the EAB's thickness and width factors, respectively. If the asteroid-pulsar collision cross-section is taken to be $\sigma_{\rm a}$, from Equation (18) of Dai et al. (2016), the collision rate is given by

$$\mathcal{R}_{\rm a} \sim \frac{\sigma_{\rm a} v_{\rm pulsar} N_{\rm a}}{V_{\rm belt}}, \quad (15)$$

where $N_{\rm a}$ is the total asteroid number in the EAB and $v_{\rm pulsar} \sim 10^7$ cm s^{-1} is the average velocity of the pulsar. Thus, the observed FRB rate reads $\mathcal{R}_{\rm FRB} \sim \zeta f \mathcal{R}_{\rm a}$ (where $\zeta = 0.24$ is the duty cycle), that is,

$$\mathcal{R}_{\rm FRB} \sim 0.33 N_{\rm a,6} f \left(\frac{\eta_{\rm t}\eta_{\rm w}}{0.25}\right)^{-1} \left(\frac{R_{\rm a,out}}{1 \ {\rm au}}\right)^{-3} \ {\rm yr^{-1}}, \quad (16)$$

where $N_{\rm a,6} = N_{\rm a}/10^6$. For FRB 180916.J0158+65, from CHIME/FRB Collaboration et al. (2020), $\mathcal{R}_{\rm FRB} \sim 25$ yr^{-1}. Inserting this observed rate into Equation (16) gives $N_{\rm a}$. Therefore, the total mass of the EAB can be approximated by

$$M_{\rm belt} \sim N_{\rm a}\bar{m} \sim 1.2 \times 10^{-2} M_\oplus \bar{m}_{18} f^{-1}$$
$$\times \left(\frac{\eta_{\rm t}\eta_{\rm w}}{0.25}\right)\left(\frac{R_{\rm a,out}}{1 \ {\rm au}}\right)^3, \quad (17)$$

where $\bar{m} = \bar{m}_{18} \times 10^{18}$ g is the average asteroidal mass. As shown in Figure 2, $R_{\rm a,out}$ is $\sim$0.13 au to $\sim$0.26 au, so the EAB's total mass $M_{\rm belt}$ is in the range of $\sim 2.6 \times 10^{-5} M_\oplus \bar{m}_{18} f^{-1} (\eta_{\rm t}\eta_{\rm w}/0.25)$ to $\sim 2.1 \times 10^{-4} M_\oplus \bar{m}_{18} f^{-1} (\eta_{\rm t}\eta_{\rm w}/0.25)$. This mass is not only about four to five orders of magnitude smaller than that of the EAB inferred from the first repeating FRB 121102 (Dai et al. 2016), but it is also comparable to the mass of the main asteroid belt in the solar system ($\sim 5 \times 10^{-4} M_\oplus$, Krasinsky et al. 2002; Li et al. 2019).

3. Discussion

We now discuss the validity and implications of our model. First, we have assumed an old-aged ($t_{\rm pulsar} \gtrsim 10^7$ yr), slowly spinning ($P_{\rm pulsar} \gtrsim 1$ s) pulsar, whose surface temperature cools as $T_{\rm s} \sim 6 \times 10^4 (t_{\rm pulsar}/10^7 \ {\rm yr})^{-1}$ K due to the fact that stellar surface blackbody radiation becomes the dominant cooling mechanism (Shapiro & Teuklosky 1983). The resultant low cooling luminosity, together with an extremely low spin-down power, makes the effects of this pulsar on any asteroid entering its magnetosphere (i.e., evaporation and ionization) become insignificant (Cordes & Shannon 2008). Thus, the asteroid can be assumed to fall freely over the stellar surface.

Second, we have also assumed the coplanarity between the binary orbit and the EAB in Section 2. This corresponds to the pulsar-EAB edge-on collision case of Dai et al. (2016). The ratio of the rate for this case to total (edge-on plus head-on) collision rate can be estimated by $\eta_{\rm t}/2$, which is $\sim$0.35 if the EAB, in structure, is analogous to the main asteroid belt in the solar system. Therefore, the probability of edge-on collisions is considerably high as compared with head-on collisions.

Third, if a binary with a pulsar and a companion star at first arose from two stars and if an asteroid belt around the companion star was outside of the critical stable circular orbit fitted by Rabl & Dvorak (1988) and Holman & Wiegert (1999), then this belt would be dynamically unstable and its orbit would be significantly changed during long-term evolution. In our model, fortunately, a wandering pulsar is captured by a star (or a white dwarf or a neutron star) surrounded by an asteroid belt and then the two objects form a binary. In this case,

numerical simulations of Smallwood et al. (2019) show that a Kuiper-belt-like outer region of the belt is highly distorted but a main-belt-like inner region remains almost unchanged for a long integration time. As $R_{a,out}$ shown in Figure 2 is in the most inner region, it would be expected that the EAB for FRB 180916.J0158+65 is dynamically quasi-stable for a period of time. How is this time estimated? Because only those asteroids swept out by the cross-section of σ_a centering around the pulsar will be accreted onto the surface of the pulsar, from Equation (15), the typical lifetime of the binary system producing repeating radio bursts can be estimated by

$$\mathcal{T}_{FRB} \sim \frac{N_a}{\mathcal{R}_a} \sim \frac{V_{belt}}{\sigma_a v_{pulsar}}$$

$$\sim 0.72 \times 10^6 \left(\frac{\eta_t \eta_w}{0.25}\right)\left(\frac{R_{a,out}}{1 \text{ au}}\right)^3 \text{ yr.} \quad (18)$$

This suggests that the lifetime $\mathcal{T}_{FRB}$ is in the range of $\sim 1.6 \times 10^3 (\eta_t \eta_w/0.25)$ yr to $\sim 1.3 \times 10^4 (\eta_t \eta_w/0.25)$ yr for $R_{a,out}$ given in Figure 2 for FRB 180916.J0158+65.

Finally, the frequency down-drift in a burst was detected to occur for FRB 180916.J0158+65 (CHIME/FRB Collaboration et al. 2020). Similarly to Wang et al. (2019) through an analysis of the movement of emitting bunches along magnetic field lines at different heights, our model can well explain the observed frequency down-drift rate and polarization (Z. N. Liu et al. 2020, in preparation).

4. Conclusions

In this Letter, we have suggested that periodic FRBs such as the recently discovered periodic FRB 180916.J0158+65 could provide a unique probe of EABs, following the pulsar-asteroid belt impact model of Dai et al. (2016), in which repeating FRBs originate from an old-aged, slowly spinning, moderately magnetized pulsar traveling through an EAB around a stellar-mass object (perhaps, a star or a white dwarf or a neutron star). It has been naturally expected that if the two objects form a binary, there should be temporally clustering and even periodically repeating bursts, as predicted in this model and implied by the early observations on the first repeating FRB 121102. We have shown that this model can be used to understand all of the observed data of FRB 180916.J0158+65, and provided some constraints on the EAB's physical properties. Our findings are as follows.

1. The outer radius of the EAB responsible for FRB 180916. J0158+65 is at least an order of magnitude smaller than that of its solar system analog.
2. The power-law index of the differential size distribution of the EAB's asteroids at small diameters (large diameters) is smaller (larger) than the corresponding index of solar system small objects.
3. The EAB's total mass is about four to five orders of magnitude smaller than that of the EAB inferred from the first repeating FRB 121102 and comparable to the mass of the main asteroid belt in the solar system.

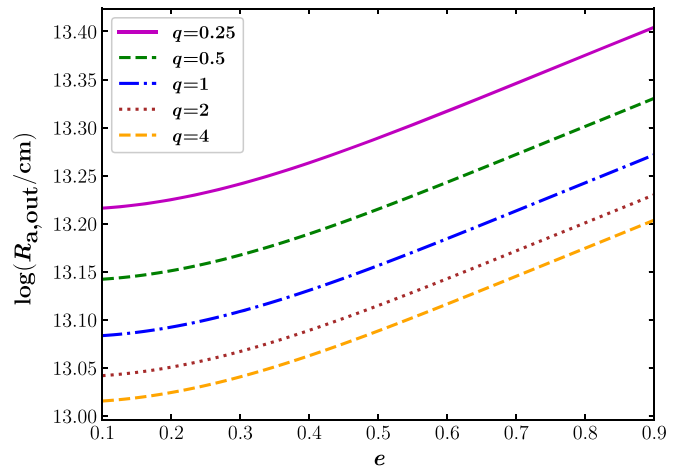**Figure 3.** $R_{a,out}$ as a function of e for $M_{pulsar} = 1.4 \, M_\odot$ and $q = 0.25, 0.5, 1, 2,$ and 4, in the case of FRB 121102 with an orbital period $P_{orb} = 159$ days and a duty cycle $\zeta = 0.47$ (taken from Rajwade et al. 2020).

Note added in proof. After the submission of this Letter, Rajwade et al. (2020) reported a periodicity search for FRB 121102 and found a tentative period of 159^{+3}_{-8} days in the periodogram with a duty cycle of $\sim 47\%$. Interestingly, this result is well consistent with the possible periodic activity predicted by our model for FRB 121102 (Dai et al. 2016; Bagchi 2017), and thus, from the analysis in this Letter, can also provide a constraint on $R_{a,out}$ of an EAB, shown in Figure 3. It is seen from this figure that $R_{a,out}$ always increases with e for a given q and is in the range of ~ 0.69 au to ~ 1.7 au, which is smaller than that of the solar system main asteroid belt by a factor of a few (DeMeo & Carry 2014; Peña et al. 2020).

ORCID iDs

Z. G. Dai ⓘ https://orcid.org/0000-0002-7835-8585

References

Bagchi, M. 2017, ApJL, 838, L16
Beloborodov, A. M. 2017, ApJL, 843, L26
Chatterjee, S., Law, C. J., Wharton, R. S., et al. 2017, Natur, 541, 58
CHIME/FRB Collaboration, Amiri, M., Andersen, B. C., et al. 2020, arXiv:2001.10275
Colgate, S. A., & Petscheck, A. G. 1981, ApJ, 248, 771
Cordes, J. M., & Chatterjee, S. 2019, ARA&A, 57, 417
Cordes, J. M., & Shannon, R. M. 2008, ApJ, 682, 1152
Dai, Z. G., Wang, J. S., Wu, X. F., & Huang, Y. F. 2016, ApJ, 829, 27
Davis, D. R., Durda, D. D., Marzari, F., Campo Bagatin, A., & Gil-Hutton, R. 2002, in Asteroids III, ed. W. F. Bottke, Jr. et al. (Tucson, AZ: Univ. Arizona Press), 545
DeMeo, F. E., & Carry, B. 2014, Natur, 505, 629
Geng, J. J., & Huang, Y. F. 2015, ApJ, 809, 24
Gourdji, K., Michilli, D., Spitler, L. G., et al. 2019, ApJL, 877, L19
Gu, W. M., Yi, T., & Liu, T. 2020, arXiv:2002.10478
Holman, M. J., & Wiegert, P. A. 1999, AJ, 117, 621
Ioka, K., & Zhang, B. 2020, ApJL, 893, L26
Ivezić, Z., Tabachnik, S., Rafikov, R., et al. 2001, AJ, 122, 2749
Kashiyama, K., & Murase, K. 2017, ApJL, 839, L3
Katz, J. I. 2016, ApJ, 826, 226
Katz, J. I. 2020, MNRAS, 494, L64
Krasinsky, G. A., Pitjeva, E. V., Vasilyev, M. V., & Yagudina, E. I. 2002, Icar, 158, 98

Kumar, P., Lu, W., & Bhattacharya, M. 2017, MNRAS, 468, 2726
Levin, Y., Beloborodov, A. M., & Bransgrove, A. 2020, arXiv:2002.04595
Li, J., Xia, Z. H., & Zhou, L. Y. 2019, A&A, 630, A68
Lin, H. N., & Sang, Y. 2020, MNRAS, 491, 2156
Lorimer, D. R., Bailes, M., McLaughlin, M. A., Narkevic, D. J., & Crawford, F. 2007, Sci, 318, 777
Lyubarsky, Y. 2014, MNRAS, 442, L9
Lyutikov, M., Barkov, M., & Giannios, D. 2020, ApJL, 893, L39
Marcote, B., Nimmo, K., Hessels, J. W. T., et al. 2020, Natur, 577, 190
Marcote, B., Paragi, Z., Hessels, J. W. T., et al. 2017, ApJL, 834, L8
Metzger, B. D., Berger, E., & Margalit, B. 2017, ApJ, 841, 14
Metzger, B. D., Margalit, B., & Sironi, L. 2019, MNRAS, 485, 4091
Murase, K., Kashiyama, K., & Meszaros, P. 2016, MNRAS, 461, 1498
Oostrum, L. C., Maan, Y., van Leeuwen, J., et al. 2020, A&A, 635, A61
Peña, J., Fuentes, C., Förster, F., et al. 2020, AJ, 159, 148
Petroff, E., Hessels, J. W. T., & Lorimer, D. R. 2019, A&ARv, 27, 4
Platts, E., Weltman, A., Walters, A., et al. 2019, PhR, 821, 1
Popov, S. B., & Postnov, K. A. 2013, arXiv:1307.4924
Rabl, G., & Dvorak, R. 1988, A&A, 191, 385
Rajwade, K. M., Mickaliger1, M. B., Stappers, B. W., et al. 2020, MNRAS, submitted (arXiv:2003.03596)
Ryan, E. L., Mizuno, D. R., Shenoy, S. S., et al. 2015, A&A, 578, A42
Scholz, P., Spitler, L. G., Hessels, J. W. T., et al. 2016, ApJ, 833, 177
Shapiro, S. L., & Teuklosky, S. A. 1983, Black Holes, White Dwarfs and Neutron Stars: The Physics of Compact Objects (New York: Wiley)
Siraj, A., & Loeb, A. 2019, RNAAS, 3, 130
Smallwood, J. L., Martin, R. G., & Zhang, B. 2019, MNRAS, 485, 1367
Spitler, L. G., Cordes, J. M., Hessels, J. W. T., et al. 2014, ApJ, 790, 101
Spitler, L. G., Scholz, P., Hessels, J. W. T., et al. 2016, Natur, 531, 202
Tong, H., Wang, W., & Wang, H. G. 2020, arXiv:2002.10265
Wang, F. Y., & Zhang, G. Q. 2019, ApJ, 882, 108
Wang, W. Y., Zhang, B., Chen, X. L., & Xu, R. X. 2019, ApJL, 876, L15
Yang, H., & Zou, Y. C. 2020, ApJL, 893, L31
Yoshida, F., & Nakamura, T. 2007, P&SS, 55, 1113
Yoshida, F, Terai, T., Ito, T., et al. 2019, P&SS, 169, 78
Zanazzi, J. J., & Lai, D. 2020, ApJL, 892, L15
Zhang, B. 2017, ApJL, 836, L32
Zhang, B. 2018, ApJL, 854, L21